Electronic supplementary information (ESI)

Sb_2S_3@Carboxyl-modified COF S-Scheme heterojunction: Sb-O-C interface enhances photocatalytic CO_2 reduction performance

Zhenfeng Zhong[a], Chenyu Zhou[a], Ming Zhu[a], Huaizhi Yang[b], Yuqi Wan[a,c], Zhiquan Pan[a], Qingrong Cheng[a,]*

[a] School of Chemistry and Environmental Engineering, Key Laboratory of Green Chemical Engineering Process of Ministry of Education, Engineering Research Center of Phosphorus Resources Development and Utilization of Ministry of Education, Wuhan Institute of Technology, Wuhan 430205, PR China

[b] School of Chemistry and Chemical Engineering, Nanjing University, Nanjing, 210033, P. R. China

[c] The Faculty of Dentistry, The University of Hong Kong, Hong Kong, 999077, PR China.

Corresponding author:

*(Q.C.) E-mail: chengqr383121@sina.com

Total number of pages: **31**

Total number of Tables: **12**

Total number of Figures: **18**

Total number of Formulas: **9**

1. Materials

Antimony trichloride ($SbCl_3$), 1,4-dioxane, p-toluenesulfonic acid (TsOH), pyruvic acid, Benzene-1,3,5-tricarbaldehyde, p-phenylenediamine were provided by McLean Reagent. Anhydrous ethanol, ethylene glycol, methanol, ethyl acetate, n-hexane, acetic acid, Mesitylene, tetrahydrofuran were provided by Sinopharm. The experimental chemicals were of analytical grade and most of the synthetic reactions used ethylene glycol.

2. Synthesis of COF-LZU-1

Weighed Benzene-1,3,5-tricarbaldehyde (32 mg, 0.05 mmol) and p-phenylenediamine (32.22 mg, 0.075 mmol) powder placed in a 10 mL vial, respectively, add anhydrous ethanol (4 mL), Mesitylene (3 mL), sonicate for 4 min, 4 min, and finally add 3 mol/L acetic acid solution (1 mL) to sonicate for 2 min. After mixing well and plugging tightly with a solid rubber stopper, the bottles were frozen in an ice-salt bath for 12 h. After freezing for 12 h, the bottles were filled with nitrogen-vacuumed three times and wrapped tightly with tinfoil. The reaction was carried out in a hydrothermal kettle at a solvent heat of 120 ℃ for 48 h and then cooled down to room temperature naturally. The obtained solid was washed with hot tetrahydrofuran and methanol for four times, then dried and stored at 60 ℃, and ground to obtain a yellow-green powder, COF-LZU-1.

3. Synthesis of COF-LC

COF-LZU-1 (100 mg), 1,4-dioxane (1 mL), Mesitylene (1 mL), 6 M aqueous acetic acid (400 μL), TsOH (40 mg of p-toluenesulfonic acid), and pyruvic acid (56 μL, 0.6 mmol) were added to the silylene vial. After ultrasonication for 20 min and freezing in an ice-salt bath for 12 h, the freezing process was followed by nitrogen filling-vacuuming three times and sealing. The reaction was heated at 120°C for 3 days to produce a precipitate and the product was isolated by suction and washed with methanol, ethyl acetate and hexane and dried under vacuum at 60°C for 24 h. Grinding yielded an orange-red powder for the COF-LC sample.

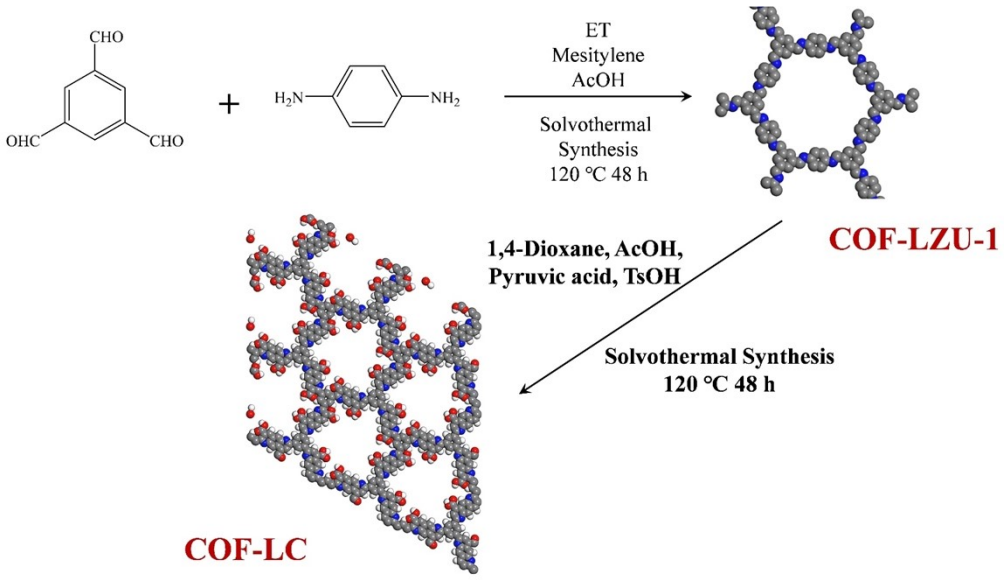

Scheme. S1 Schematic diagram of the COF-LC synthesis route.

4. Synthesis of Sb_2S_3

0.724 g of $SbCl_3$ were added to 80 mL of ethylene glycol and then magnetically stirred for 1 h. Then 1.4 g of thiourea was added to the above solution and stirred continuously to obtain a clarified solution. Subsequently, the obtained solution was kept in a reactor at 180 ℃ for 10 h. After reaching room temperature, the product was collected by centrifugation, rinsed several times with anhydrous ethanol and deionized water, and dried at 60 ℃ for 12 h. The black powder was obtained as Sb_2S_3.

5.Instrumentation

The surface and internal morphology were imaged by means of scanning electron microscopy (SEM, Gemini SEM 300, Carl Zeiss, Germany) and high-resolution transmission electron microscopy (TEM, Titan G260-300, FEI, USA), respectively. TEM was utilised in conjunction with Energy Dispersive X-ray Spectrometry (EDS) to obtain elemental mapping images. Powder X-ray diffraction (P-XRD) patterns were measured employing a Rigaku MiniFlex600 from Japan over a test range of 2-90° at a scan rate of 1° min^{-1}. FTIR spectroscopic analysis was performed in the 4000 - 400 cm^{-1} range using a Scientific Nicolet iS 20 spectrometer (Thermo Fisher, USA) with KBr as a background. UV-Vis diffuse reflectance (UV-Vis DRS) absorption spectra were recorded using a Shimadzu UV spectrometer (UV-3600i Plus) with an integrating sphere attachment. Using $BaSO_4$ as the reflectance standard, the analysis range is from

200 nm to 800 nm. A K-Alpha spectrometer (Thermo Scientific, USA) equipped with an Al Kα X-ray source (hν = 1486.6 eV) was used to obtain X-ray photoelectron spectra (XPS). The N_2 adsorption-desorption isotherm was measured at 393.15 K using an ASAP 2460 instrument from Micromeritics (USA) and was interpreted using the Brunner-Emmett-Taylor (BET) equation. The Barret-Joyner-Halenda (BJH) model was used to generate the pore size distribution maps. The activated species were measured by analysis of electron spin resonance (ESR) spectra using a Bruker EMXPLUS-6/1 spectrometer from Germany. Zeta potentials were obtained using a Malvern Zetasizer Nano ZS90, UK. Fluorescence spectra (FL) were tested using the Edinburgh FLS1000 in the UK, and the emission peak under 468 excitation was used as the monitoring wavelength when testing the lifetime.

6. Photoelectrochemical measurements

Electrochemical impedance spectroscopy (EIS), transient photocurrent (TPC), and Mott-Schottky (M-S) curve tests were conducted on a normal three-electrode system with an electrochemical analyzer (CS Studio 6, Corr Test, China). As counter and reference electrodes, Pt and Ag/AgCl electrodes were chosen. A solution containing 5 $mmol \cdot L^{-1}$ $K_3[Fe(CN)_6]$ and 0.1 $mol \cdot L^{-1}$ KCl was used as the electrolyte for the EIS test. The M-S and TPC tests utilised an aqueous solution of 0.5 $mol \cdot L^{-1}$ Na_2SO_4 as the electrolyte and a 300W xenon lamp as the light source. The pH of the solution was 6.85.

7. Photocatalytic degradation experiment

A 300 W Xenon lamp was employed as an emulated solar light source. The degradation process of Methylene Blue (MB) is employed as an illustrative example:

During the photocatalytic degradation experiment, 10mg of sample powders and 50mL MB ($30mg \cdot L^{-1}$) aqueous solution were introduced into the quartz reactor while being stirred magnetically. The mixture was continuously magnetically stirred for 1 h to achieve adsorption-desorption equilibrium in the absence of light prior to the photoreaction. Upon sunlight exposure, 3 mL of sample was taken from the suspension every 10 minutes up to 60 minutes. The absorption spectrum of MB was measured using the UV spectrophotometer (UV-2450, Shimadzu, Japan) from the supernatant liquid of each sample. The photocatalysts were filtered out through a 0.22 μm Millipore filter (aqueous phase) before each measurement. Then the degradation rate of CIP could be calculated by the following formula (**Eq. S1**):

$$Degradation\ rate\ (DR,\ \%) = (C_0 - C_t)/C_0 \times 100\% \quad (1)$$

where C_0 represents the absorbance value of the initial concentration of CIP achieved at adsorption-desorption equilibrium, and C_t represents the concentration at a specific irradiation time. The maximum absorbance of MB was determined at a wavelength of 664 nm. Consequently, the photocatalytic degradation activity of other pollutants could be measured by these similar steps.

8. Photocatalytic cyclic degradation experiment

The photocatalytic cyclic degradation experiment was conducted using the semi-permeable membrane method, utilizing 30 mg of photocatalyst. The sample was kept after adsorption-desorption equilibrium, and the ultimate sample was acquired following 60 min of irradiation. This whole process constitutes one cycle. Rinse the remaining MB on the membrane surface lightly with DI water and dry as much as possible overnight at 60 ℃. Then, the following day, 50 mL of fresh 30 $mg \cdot L^{-1}$ MB solution was added and a new round of the photocatalytic degradation test was started. These experimental parts were repeated five cycles for a total of 8 hours.

9. Photocatalytic free radicals capture experiment

The procedure for the photocatalytic trapping experiments was basically the same as for the photocatalytic degradation experiment. The only difference is that various scavengers for distinct active species were introduced into the reactor 10 seconds before the lamp irradiation and kept the sample intact in time.

10. Photocatalytic CO_2 reduction experiment

The photocatalytic CO_2 reduction reaction was carried out in a 110 mL cylindrical sealed quartz reactor. The light source was a 300 W xenon lamp (light intensity 1000 mW/cm^2).30 mg of photocatalyst, and 50 mL of mixed solution (using the volume ratio of the three solutions mixed, H_2O: MeCN: TEOA=1:3:1) were mixed and dispersed by ultrasonication for 10 min. The reactor system was purged with CO_2 for at least 20 minutes to ensure that the air in the reactor was completely replaced by CO_2 and that the internal partial pressure was 0.04 MPa. In this, the sample was homogeneously

suspended in the reactor and magnetically stirred. During the photocatalytic experiments, 300 μL of gas was extracted from the reactor every hour with a syringe needle and quantified by a gas chromatograph (GC9790II, China). The CO produced is determined by gas chromatography and the CO output rate can be calculated using the following formula (**Eq. S2**):

$$\text{CO production rate} = \text{amount of CO (μmol)} / \left[5\ (\text{h})^{*}\ m_{sample}\ (\text{g})\right] \left(\mu\text{mol} \cdot \text{h}^{-1} \cdot g^{-1}\right) \quad (2)$$

11. Photocatalytic cyclic CO_2 reduction experiment

The photocatalytic cyclic CO_2 reduction test was repeated the experimental steps described above for five cycles.

12. Isotope tracer experiment

Isotope tracer experiments were conducted using either $^{13}CO_2$ (99% purity) or $^{12}CO_2$ as reactant under standard reaction conditions. After a 4-hour reaction, 300 μL gas in the head space was injected into a Shimadzu GCMS QP2010.

13. Theoretical calculation method

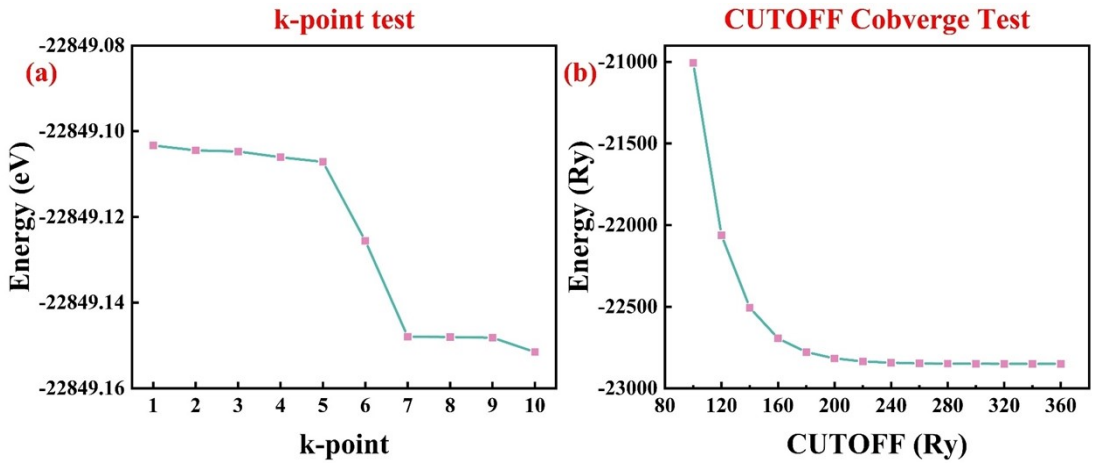

Fig. S1 (a) k-point test; (b) Convergence test for cut-off energy

Theoretical computations utilizing the CASTEP module within the Materials Studio software apply the GGA-PBE (Generalized Gradient Approximation-Perdew Burke Ernzerhof) function. In this paper, the geometrical optimisation conditions for Sb_2S_3 and COF-LC are as follows, with the k-points set to 3 × 3 × 3 (**Fig.S1a**) and 1 × 1 × 1, respectively. The cut-off energy was set to 320 eV (**Fig.S1b**). The convergence tolerance parameter for the maximum step size is 0.001 Å, the maximum force is 0.01 eV/Å, the energy change is 1.0×10^{-6} eV/atom, and the maximum stress is 0.05 GPa. In the surface structure calculations, a 15 Å vacuum layer was constructed to eliminate interactions between the periodic structures of the surface model, and all of the above calculations have been tested for convergence.

14. TR-PL

The TR-PL decay spectra curves were fitted by the biexponential decay kinetics function expressed as **Eq. (3)**:

$$I(t) = B_1 e^{-t/\tau_1} + B_2 e^{-t/\tau_2} \qquad (3)$$

Meanwhile, the average lifetime τav was determined using the **Eq. (4)** :

$$\tau_{av} = \left(B_1\tau_1^2 + B_2\tau_2^2\right) / \left(B_1\tau_1 + B_2\tau_2\right) \qquad (4)$$

The τ_1 and τ_2 were the short and long lifetimes, which was mainly contributed by the radiative pathways and reflected the nonradiative process, respectively. The Kent was the rates of the non-radiative transfer, which can be calculated according to the **Eq.5**:

$$K_{ent} = \tau_1^{-1} - \tau_2^{-1} \qquad (5)$$

The parameters and results of fluorescence lifetime calculation are shown in **Table S6**.

15. DFT calculation of photogenerated carrier mobility

The carrier mobility is derived from the deformation potential theory as **Eq.6**:

$$\mu = \left(2e\hbar^3 C_{2D}\right) / \left(3K_B T \left|m^*\right| E_d^2\right) \qquad (6)$$

where ħ, K_B and T are the approximate Planck's constant, Boltzmann's constant and temperature, respectively, and m*, E_d and C_{2D} are the effective mass, the deformation potential constant and the elasticity constant of the 2D material, respectively. Stresses were selected as 99%, 99.5%, 100%, 100.5%, 101%.

16. AQY calculation section

The apparent quantum yield (AQY) of the photocatalyst was calculated using the **Eq.7**:

$$AQY(\%) = the\ number\ of\ reacted\ electrons / the\ number\ of\ incident\ electrons \times 100\% \quad (7)$$

Namely：

$$AQY(\%) = N_e / N_p \times 100\%$$
$$= \left[10^9 (\nu \times N_A \times K) \times (h \times c)\right] / \left[(I \times A \times \lambda)\right] \times 100\% \quad (8)$$

v= CO generation rate

N_A= Avogadro number = 6.02×10^{23}

K= Number of electrons transferred by the reaction

K_{CO}= 2 [1]

K_{H2}=2 [2]

h = 6.626×10^{-34} J/s

c= 3×10^8 m/s

I = Optical power density ($W\cdot m^2$)

A= Incident light area (m^2)

λ= wavelength (nm)

Table S1 The amount of various raw materials in the composite synthesis (SSLC-x (x=1-3)).

heterojunction-x	Sb_2S_3 (g)	COF-LC (g)
SSLC-1 $_{(1:1)}$	0.050	0.050
SSLC-2 $_{(2:3)}$	0.050	0.075
SSLC-3 $_{(3:7)}$	0.050	0.117

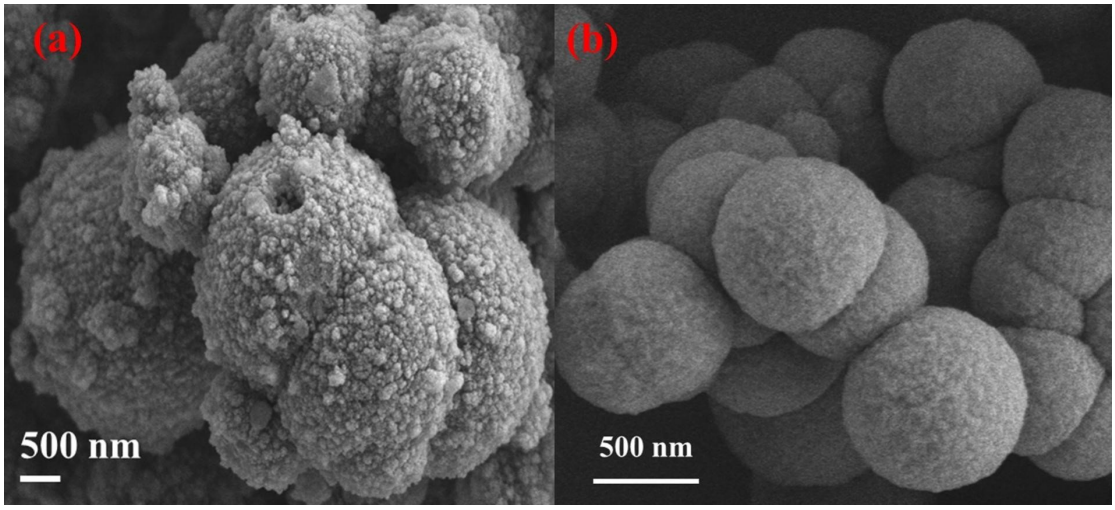

Fig. S2 Before and after modification COF-LC(a) and LZU-1(b).

Table S2 The energy dispersive spectrum (EDS) of the SSLC-2 photocatalyst.

ELEMENT	[NORM. WT. %]	[NORM. AT. %]
CARBON	23.82	58.10
NITROGEN	3.66	7.66
OXYGEN	2.11	3.86
ANTIMONY	50.44	12.13
SULFUR	19.97	18.25
SUM:	100	100

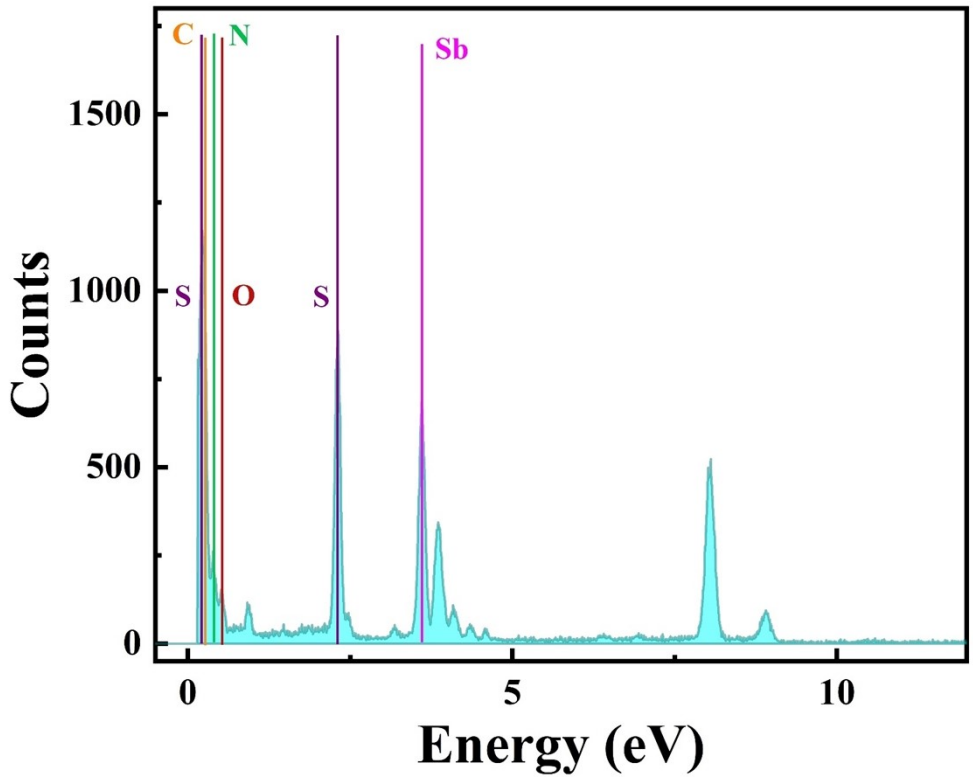

Fig. S3 The EDS element content data of photocatalyst SSLC-2.

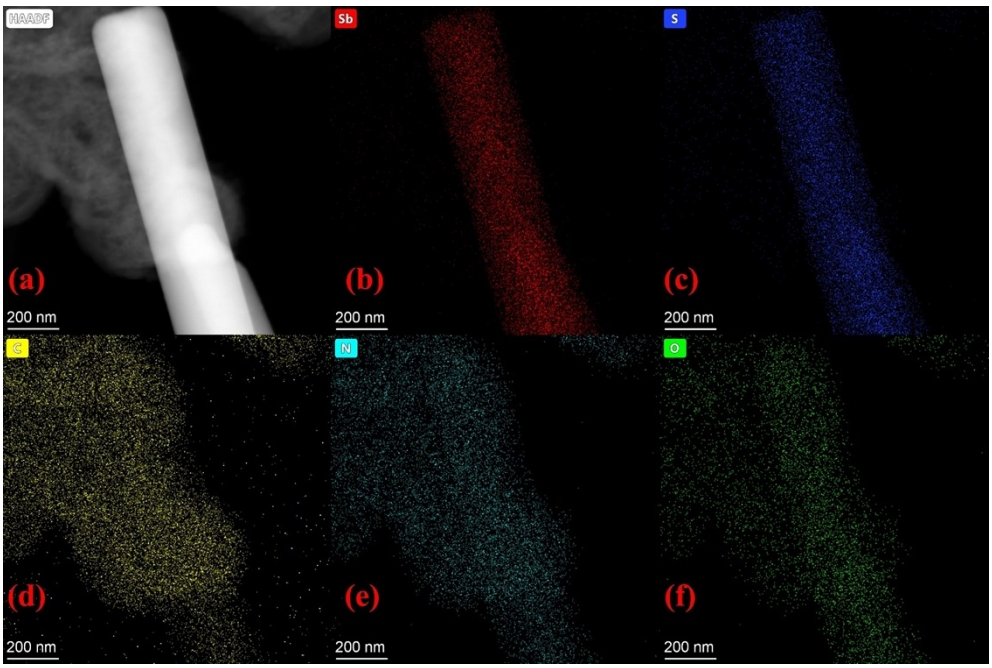

Fig. S4 The EDX spectroscopy mapping images of (a) HAADF of SSLC-2, (b) Sb, (c) S, (d) C, (e) N, (f) O elements.

Table 3 Zeta potential values of three monomers at different pH solutions

Sample	pH value	Potential average (mV)
Sb_2S_3	3	39.73
	7	21.53
	10	-10.51
COF-LC	3	-30.73
	7	-18.43
	10	33.00

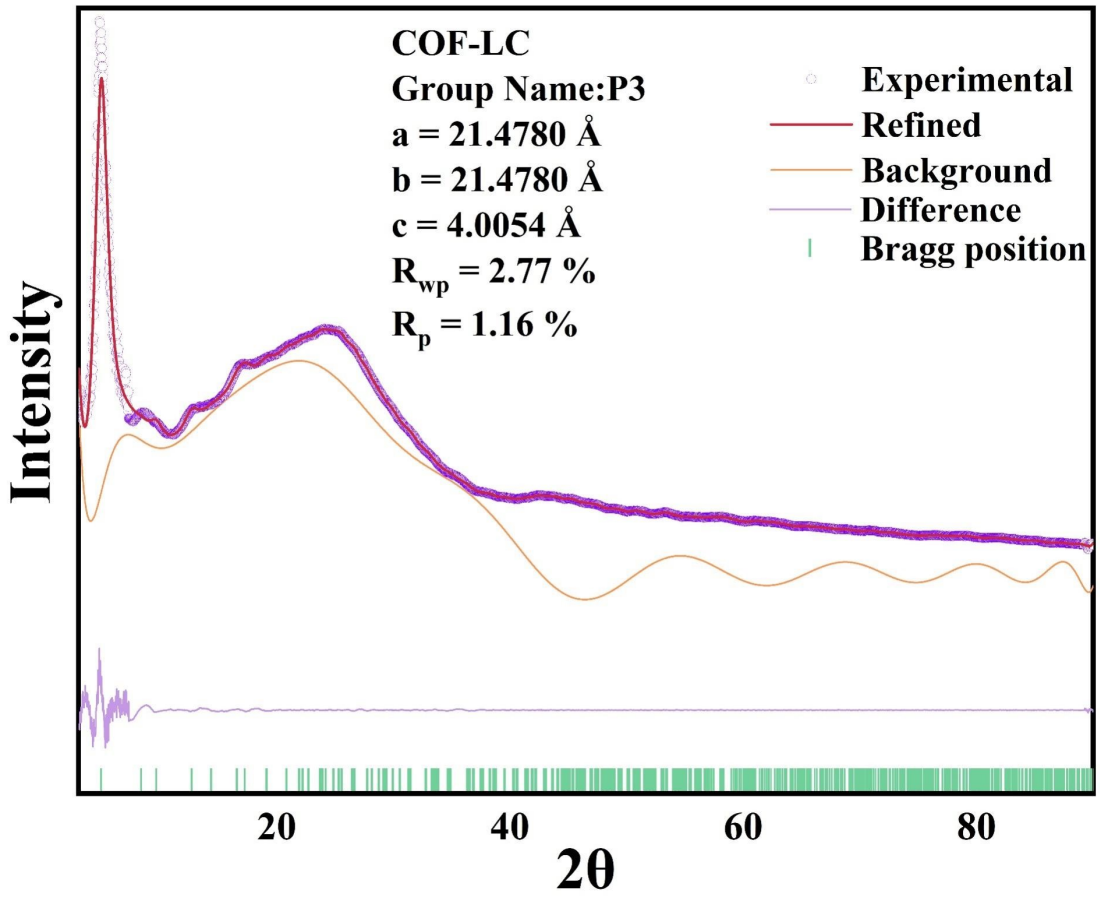

Fig. S5 Experimental and simulated PXRD patterns of COF-LC.

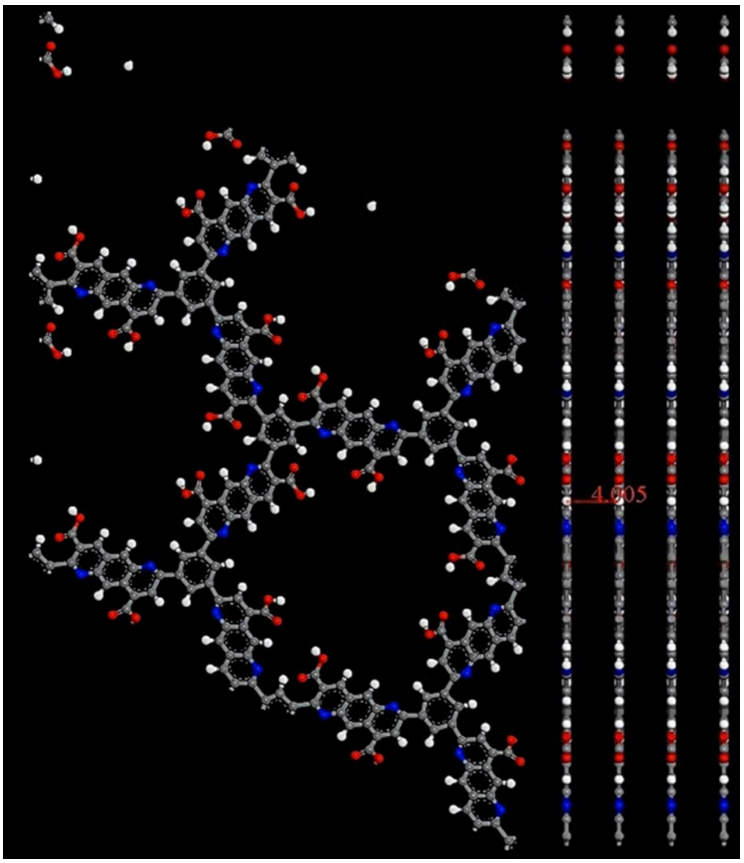

Fig. S6 Structure of COF-LC

Table S4 BET quantitative results of specific surface area and porosity distribution of 4 catalysts

	Sb_2S_3	COF-LZU-1	COF-LC	SSLC-2
The specific surface areas (m^2/g)	1.25	32.42	79.73	96.02
Adsorption average pore diameter (4V/A) (mg)	12.80	16.30	6.51	7.28

Table S5 The elements values and error (%) of selected equivalent circuits for EIS.

SAMPLE/VALUE	Rs (Ω)	Rct (Ω)	CPE1-T	CPE1-P
Sb_2S_3	8.708	2610.20	8.129E-5	0.784
ERROR (%)	1.438	3.471	0.791	0.494
LZU-1	9.998	3208.70	7.646E-5	0.736
ERROR (%)	2.134	3.424	0.978	0.625
COF-LC	8.203	1714.90	8.056E-5	0.869
ERROR (%)	1.400	3.849	1.139	0.705
SSLC-1	17.186	547.55	8.046E-5	0.812
ERROR (%)	0.547	2.171	0.626	0.564
SSLC-2	17.692	223.08	4.043E-5	0.809
ERROR (%)	0.827	1.299	0.979	0.827
SSLC-3	15.474	928.86	9.218E-5	0.707
ERROR (%)	1.486	5.786	1.384	1.323

Table S6 Time-resolved fluorescence decay parameters of COF-LC, Sb_2S_3 and SSLC-2 samples.

SAMPLE	Lifetime τ (ns)	Pre-exponential factors B%	Average lifetime τ_{av} (ns)	x^2	K_{ent} (ns^{-1})
COF-LC	τ_1=*0.7704* τ_2=3.2827	B_1=65.55 B_2=34.45	1.6359	0.8059	0.9934
Sb_2S_3	τ_1=*0.2058* τ_2=8.8134	B_1=85.65 B_2=14.35	1.4411	0.9253	4.7456
SSLC-2	τ_1=*0.2409* τ_2=5.2634	B_1=94.29 B_2=5.71	0.5278	0.9436	3.9611

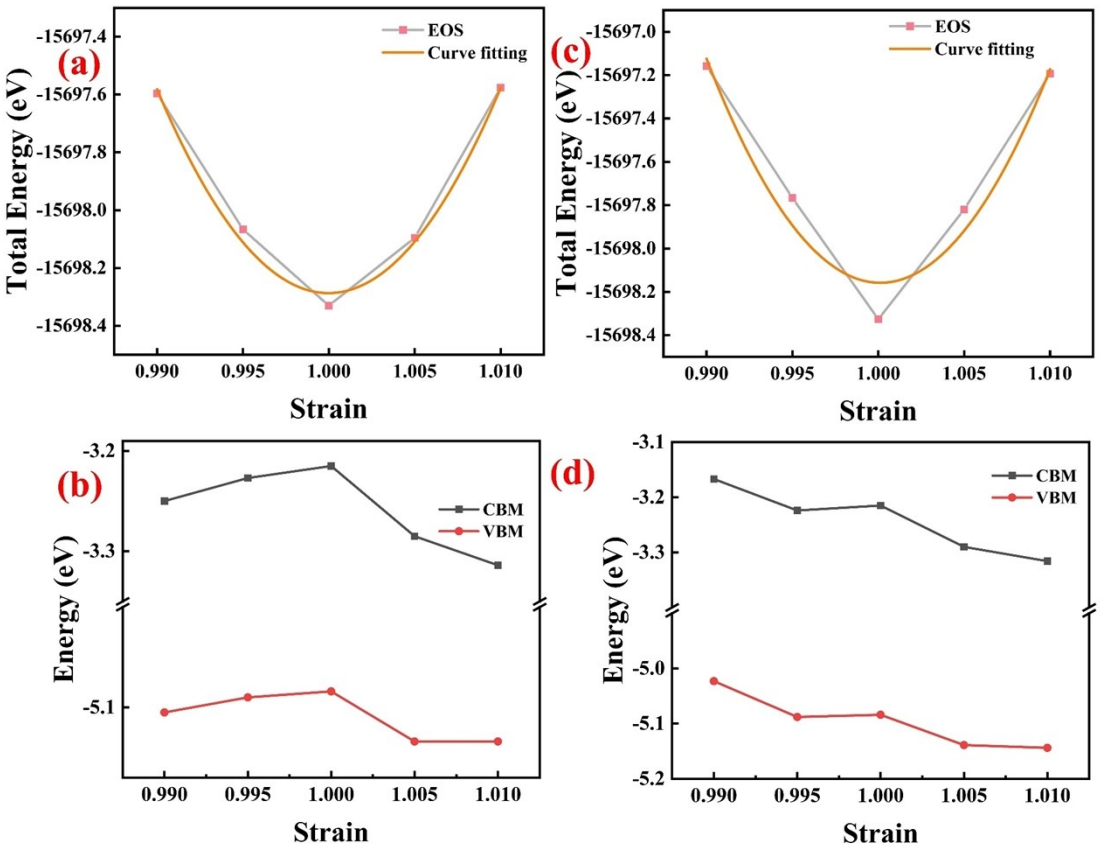

Fig. S7 Calculation parameters related to COF-LC.

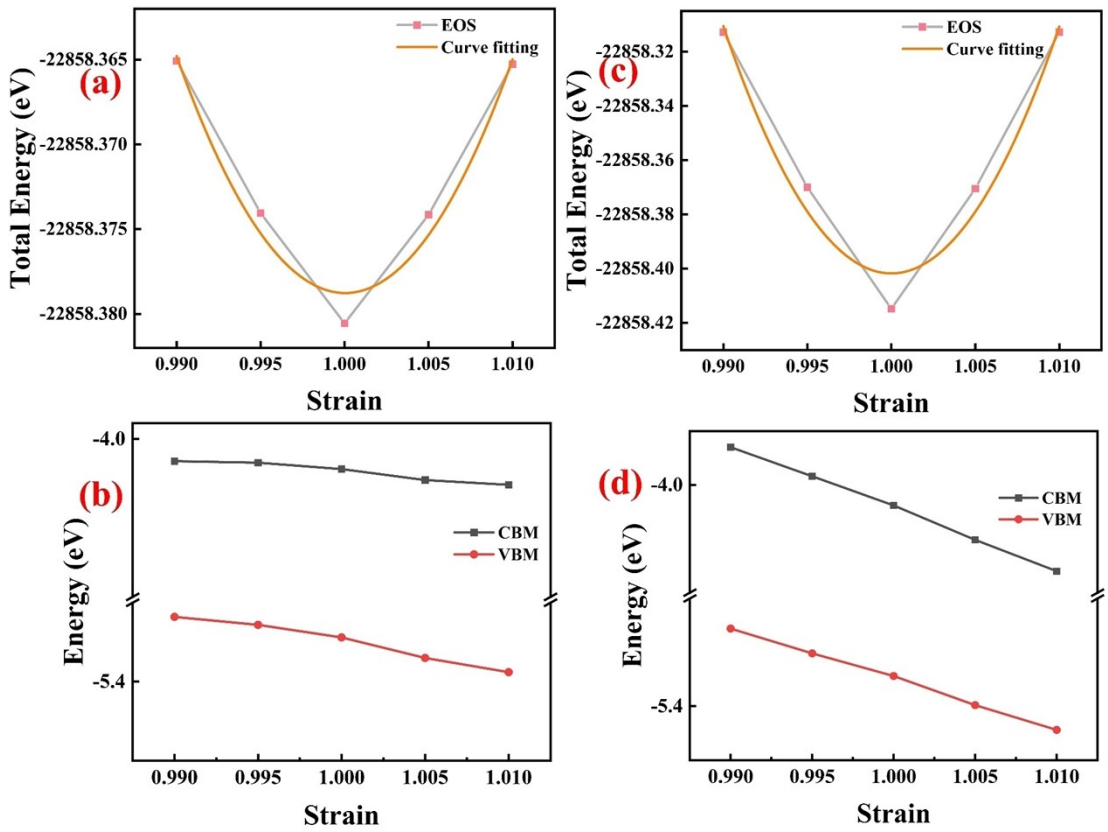

Fig. S8 Calculation parameters related to Sb_2S_3.

Table S7 Effective masses (m_e*), deformation potential constants (E_d, eV), elastic constants (C_{2D}, $N \cdot m^{-1}$) and carrier mobilities (μ_{2D}, $cm^2 \cdot V^{-1} \cdot s^{-1}$) along the a-direction for both h^+ and e^- in a monolayer of X(X=Sb_2S_3, COF-LC).

System	Directional	Carriers	m_e^* (m_0)	E_d (eV)	C_{2D} ($N \cdot m^{-1}$)	μ_{2D} ($cm^2 \cdot V^{-1} \cdot s^{-1}$)
Sb_2S_3	*x*	h^+	2.628	-4.07	121.4665	17.1648
		e^-	4.2475	-4.42		4.8929
	y	h^+	2.4260	-4.72	810.6349	61.9115
		e^-	4.1841	-5.78		13.8803
COF-LC	*x*	h^+	2.6494	-2.04	7079.7741	272.9267
		e^-	3.8843	-3.72		38.1865
	y	h^+	2.6434	-1.36	10098.5602	879.9046
		e^-	3.8755	-3.06		80.8648

Table S8 Photocatalytic CO_2 reduction performance and selectivity of different samples.

Sample	Selectivity (%)		Yield (μmol·g^{-1}·h^{-1})	
	CO	H_2	CO	H_2
Sb_2S_3	98.17	1.82	13.95	0.26
LZU-1	98.85	1.15	27.99	0.33
COF-LC	99.54	0.46	176.69	0.82
SSLC-1	99.83	0.17	627.16	1.09
SSLC-2	99.71	0.29	831.74	2.40
SSLC-3	99.70	0.30	528.54	1.61

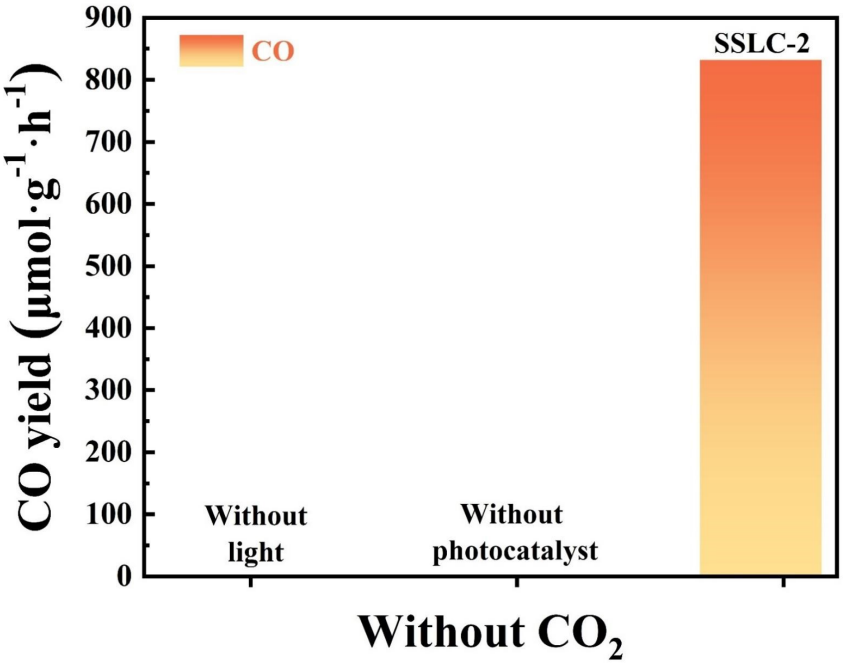

Fig. S9 The control experiments that CO formation under different conditions on SSLC-2.

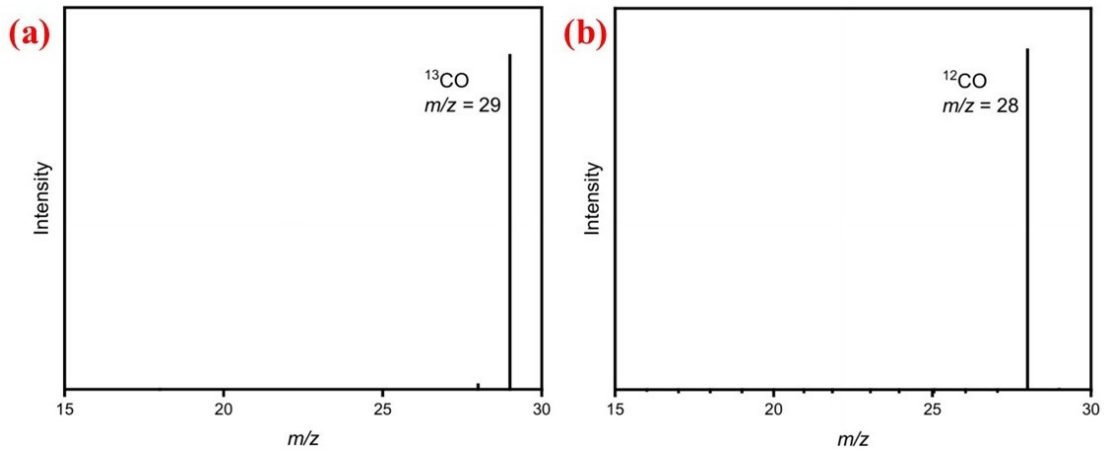

Fig. S10 MS spectra of ^{13}CO (top) and ^{12}CO (bottom) after CO_2 RR using $^{13}CO_2$ and $^{12}CO_2$, respectively.

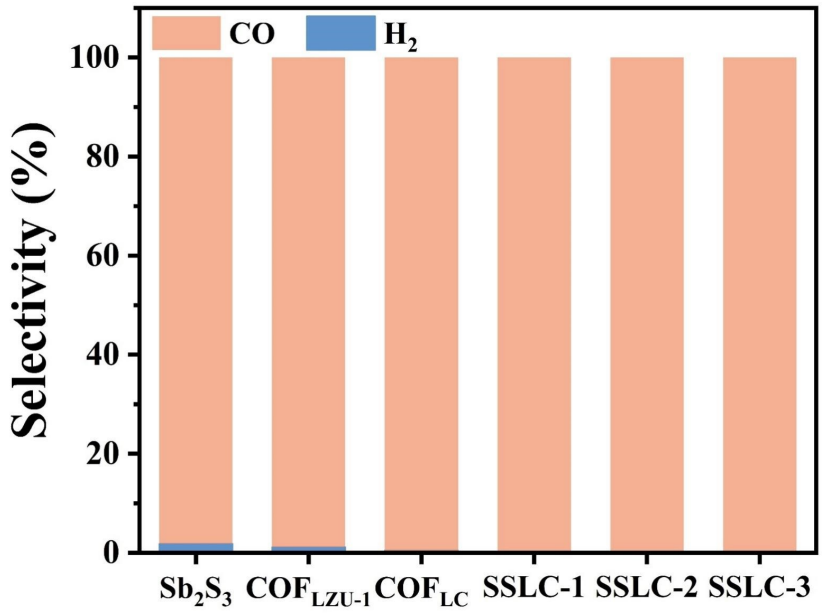

Fig. S11 The selectivity of CO and H_2.

Table S9 The AQY values for different samples irradiated at the same wavelength to produce CO and H_2.

Photocatalyst	**H_2 production (μmol)**	**CO production (μmol)**	**AQE (%)**	
			H_2	CO
Sb_2S_3	0.26	13.95	0.003	0.177
LZU-1	0.33	27.99	0.004	0.356
COF-LC	0.82	176.69	0.010	2.247
SSLC-1	1.09	627.16	0.014	7.975
SSLC-2	2.40	831.74	0.031	10.576
SSLC-3	1.61	528.54	0.020	6.721

Table S10 Comparison of photocatalytic CO_2 reduction: CO yield of different photocatalysts.

Sample	Light source	Activity ($\mu mol \cdot g^{-1} \cdot h^{-1}$)	Selection (%)	Reference
ZnZn-Salen-COF	300 W Xe lamp	102.10		3
$Cs_4Mn(Bi_{1-x}Sb_x)_2Cl_{12}$	300 W Xe lamp	35.10	100.00	4
30%-Sb/g-C_3N_4	300 W Xe lamp	2.03		5
$Cs_3Sb_2I_9$	300 W Xe lamp	95.70	96.96	6
CoBi@N-GC-10%-7	300 W Xe lamp	44.09	55.00	7
SSLC-2	300 W Xe lamp	831.74	99.71	This work
Coembedding plasmonic Au nanocrystals	visible-light	84.70	25.45	8
DPC-C4-Ni	solar light	2464	95.00	9

The reduction units of the last two substances are: $mmol \cdot g^{-1} \cdot h^{-1}$

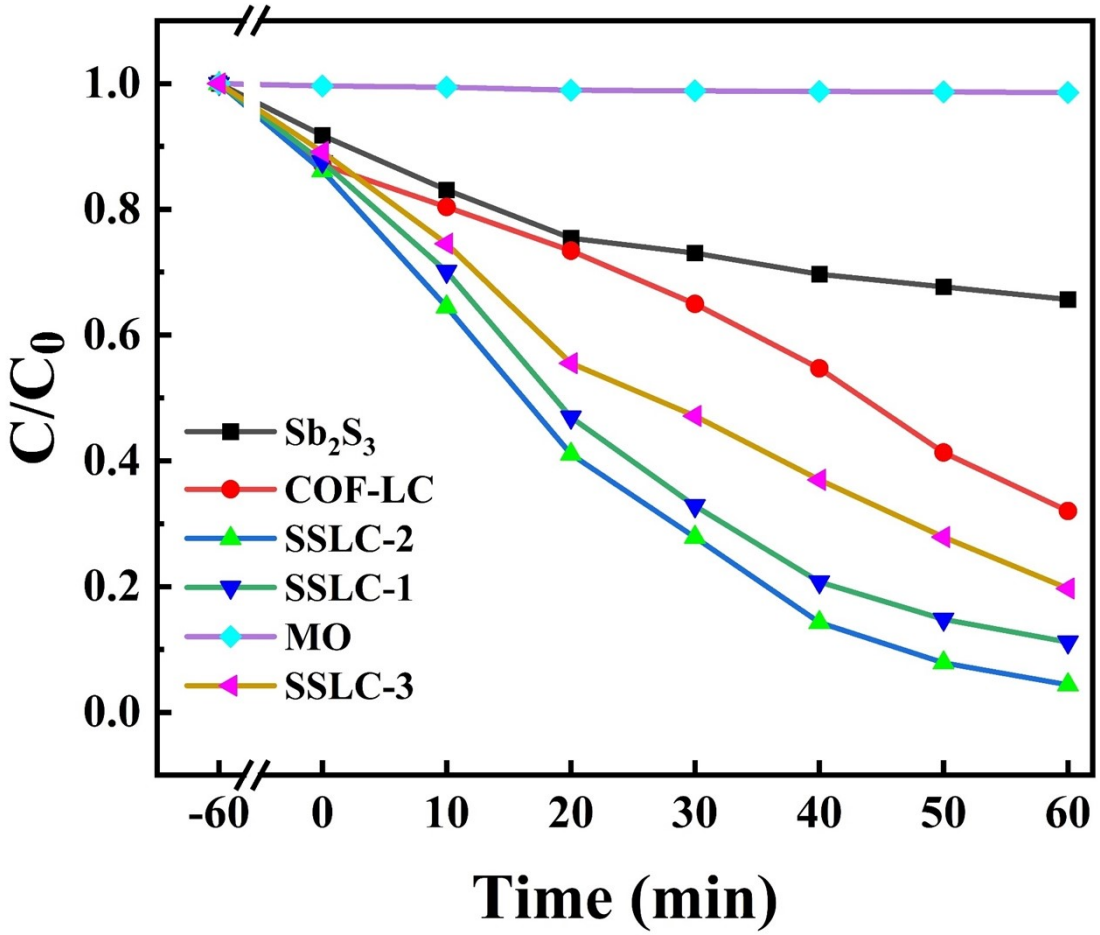

Fig. S12 Photocatalytic degradation rate of SSLC-2 on 20 mg·L^{-1} MO under visible light irradiation.

Table S11 Comparison of SSLC-2 heterojunction with other catalysts for photocatalytic degradation of MB under UV-visible irradiations.

Sample/mg	V (mL) / C_0 ($mg \cdot L^{-1}$)	Time (min)	Light source	Result (%)	TOF	Ref
BSTO/25	50/10	180	sunlight	77.30	0.0858	[10]
Sb_2S_3/SiO_2 /25	50/6	120	Visible light	92.50	0.0925	[11]
Bi_2S_3/Sb_2S_3/30	50/10	30	Visible light	94.33	0.5241	[12]
$CoNi_2S_4/MoS_2$ /20	100/10	90	Visible light	100.00	0.5555	[13]
25 wt. % Sb_2S_3/α-Ag_2WO_4 / 50	100/20	60	Visible light	91.23	0.6082	[14]
SSLC-2/10	50/30	60	Visible light	93.15	2.3288	This work

TOF is calculated according to an equation:

$$TOF = \left(C_0 \times V_{TC} \times \text{Degradation rate}\right) / \left(m_{\text{catalyst}} \times t\right) \quad (9)$$

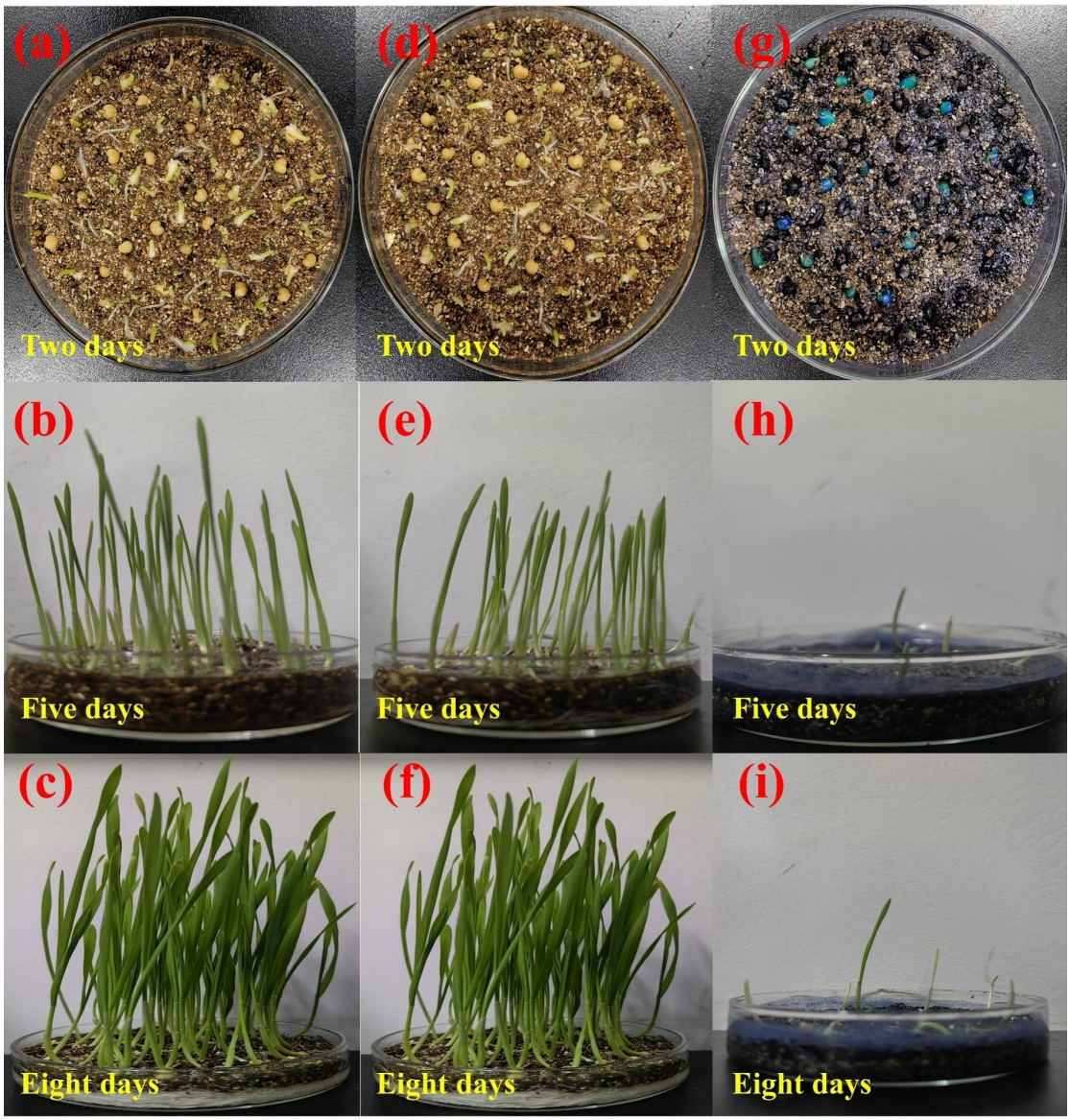

Fig. S13 Growth of wheat seeds in (a, b, c) tap water; (d, e, f) MB-containing solutions and (g, h, i) photocatalytic treatment solutions.

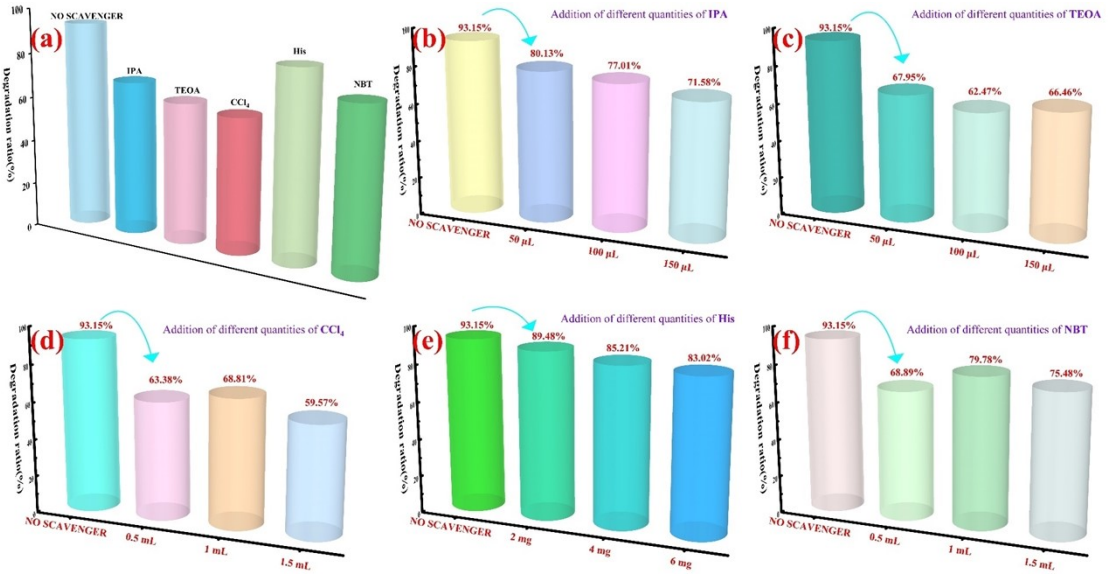

Fig. S14 (a)The radical trapping test of SSLC-2 by different scavengers; (b) IPA; (c) TEOA; (d) CCl4; (e) His; (f) NBT.

Table S12 Partly displayed XPS binding energy data corrected by C 1s level at 284.8 eV plus correspond to FWHM value.

SAMPLE	ELEMENT	DATA	CORRECTION DATA	FWHM (EV)
Sb_2S_3	Sb 3d	528.89	528.85	0.98
COF-LC	O 1s	531.51	531.39	1.72
SSLC-2	Sb 3d	529.68	529.84	1.45
	O 1s	529.68	529.84	1.45

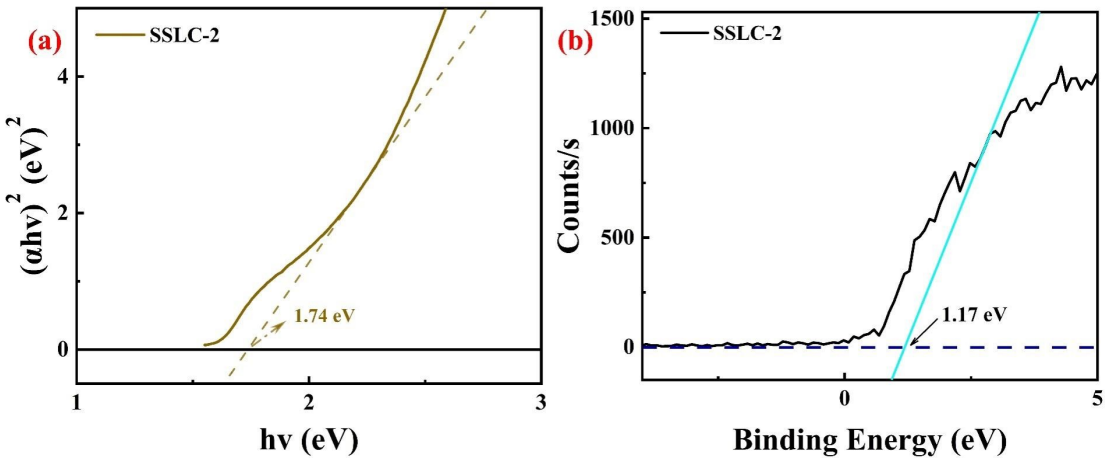

Fig. S15 (a) Band gap value and (c) valence band value of SSLC-2.

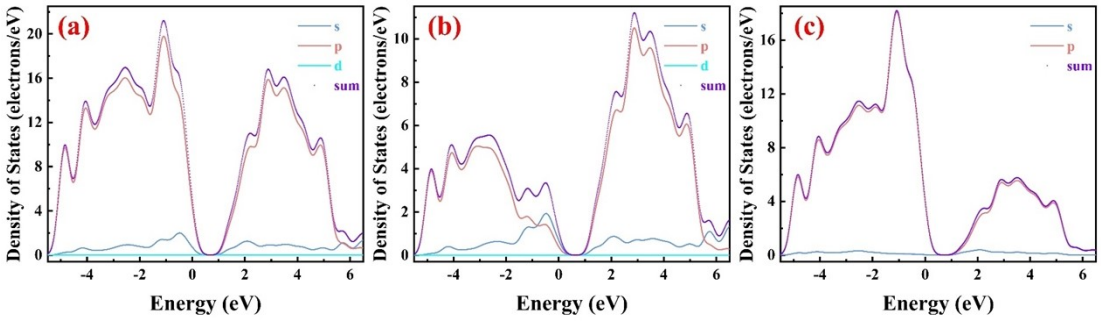

Fig. S16 PDOS plots of Sb_2S_3 (a) general; (b) Sb; (c) S.

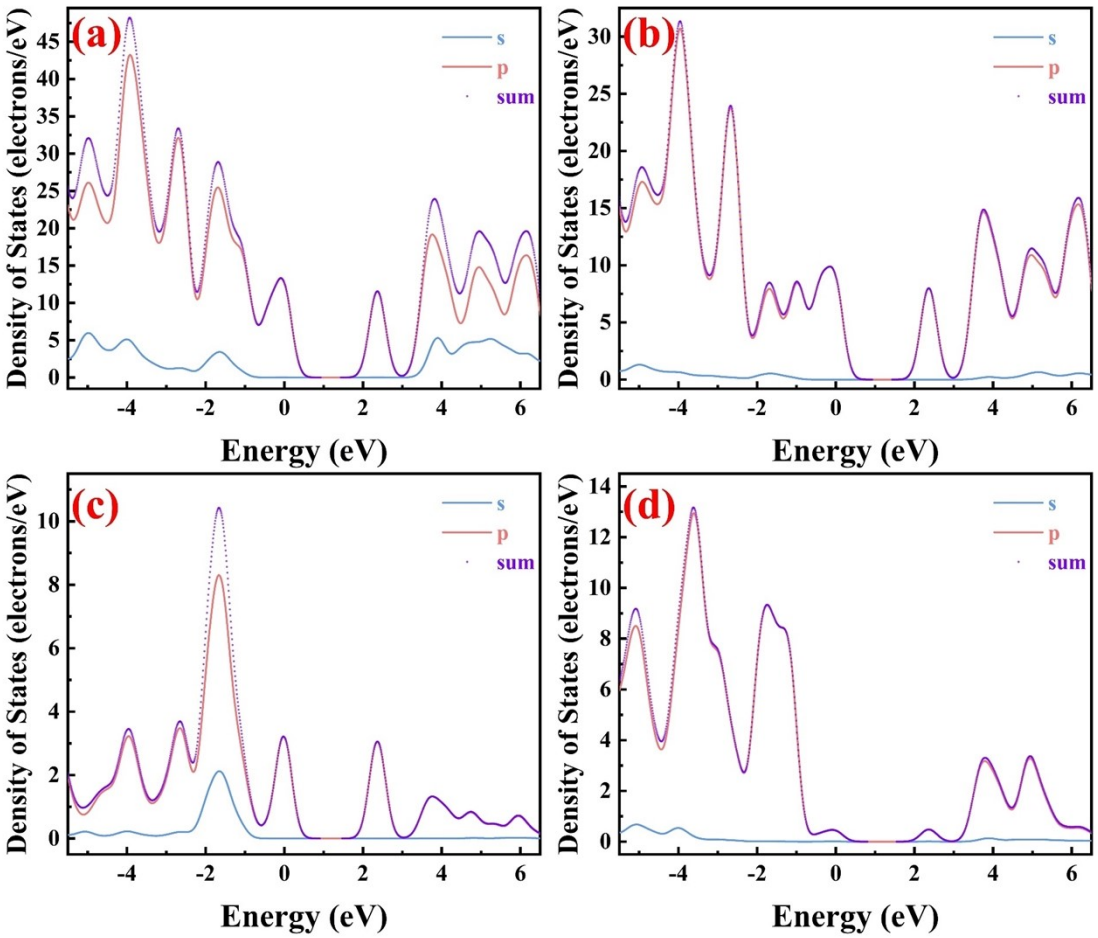

Fig. S17 PDOS plots of COF-LC (a) general; (b) C; (c) N; (d) F.

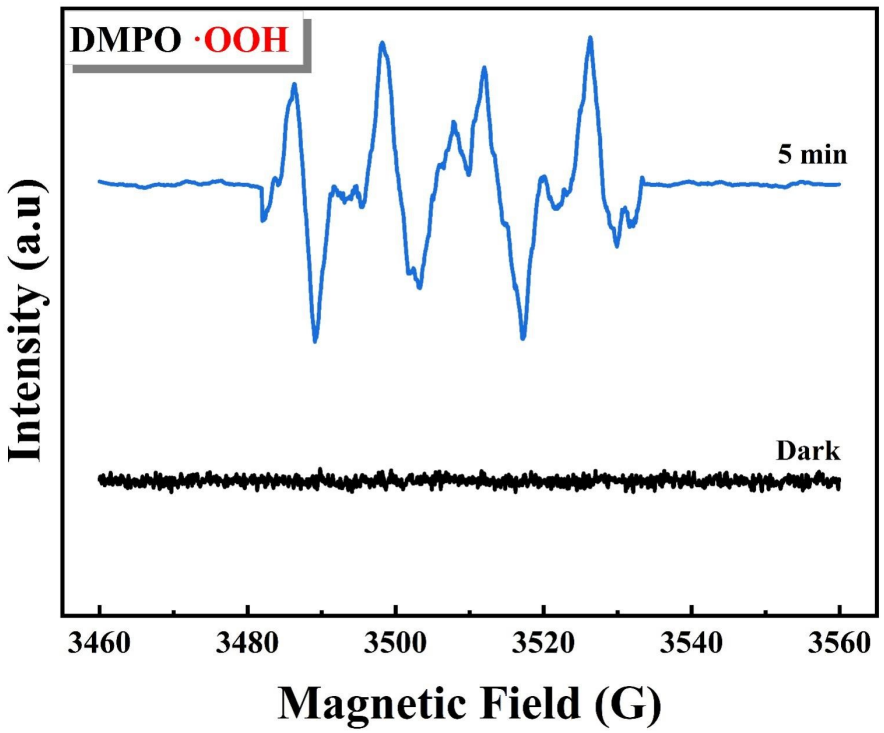

Fig. S18 ESR spectra of SSLC-2 heterojunction in dark and light.

References

1. L. Cheng, X. Yue, L. Wang, D. Zhang, P. Zhang, J. Fan and Q. Xiang, *Advanced Materials*, 2021, **33**, 2105135.
2. H. Lin, K. Zhang, G. Yang, Y. Li, X. Liu, K. Chang, Y. Xuan and J. Ye, *Applied Catalysis B: Environmental*, 2020, **279**, 119387.
3. H. Dong, L. Fang, K. X. Chen, J. X. Wei, J. X. Li, X. Qiao, Y. Wang, F. M. Zhang and Y. Q. Lan, *Angewandte Chemie International Edition*, 2024, DOI: 10.1002/anie.202414287.
4. H. Wei, Z. Li, H. Wang, Y. Yang, P. Cheng, P. Han, R. Zhang, F. Liu, P. Zhou and K. Han, *Journal of Energy Chemistry*, 2023, **82**, 18-24.
5. J. Zhang, J. Fu and K. Dai, *Journal of Materials Science & Technology*, 2022, **116**, 192-198.
6. Y. Wang, Q. Zhou, Y. Zhu and D. Xu, *Applied Catalysis B: Environmental*, 2021, **294**.
7. F. Lv, L. He, X. Bai, D. Wang and Y. Zhao, *Journal of Colloid and Interface Science*, 2024, **675**, 1069-1079.
8. J. Dong, Z. Yang, H. Li, Y. Li and J. Wei, *Journal of the American Chemical Society*, 2025, DOI: 10.1021/jacs.5c13007.
9. R. Verma, R. Belgamwar, P. Chatterjee, R. Bericat-Vadell, J. Sa and V. Polshettiwar, *ACS Nano*, 2023, **17**, 4526-4538.
10. M. S. Patil, N. Kitchamsetti, S. R. Mulani, S. R. Rondiya, N. G. Deshpande, R. A. Patil, R. W. Cross, N. Y. Dzade, K. K. Sharma, P. S. Patil, Y.-R. Ma, H. K. Cho and R. S. Devan, *Journal of the Taiwan Institute of Chemical Engineers*, 2021, **122**, 201-209.

11. S. Sharma and S. Basu, *Journal of Cleaner Production*, 2021, **280**.
12. X. Li, K. Yang, F. Wang, K. Shi, W. Huang, K. Lu, C. Yu, X. Liu and M. Zhou, *Journal of Alloys and Compounds*, 2023, **953**.
13. B. R. Anusha, Udayabhanu, S. Appu, F. Alharethy, G. Srinivas Reddy, Abhijna, M. A. Sangamesha, G. Nagaraju, S. Girish Kumar and K. Prashantha, *Journal of Physics and Chemistry of Solids*, 2025, **198**.
14. C. Ayappan, V. Jayaraman, B. Palanivel, A. Pandikumar and A. Mani, *Separation and Purification Technology*, 2020, **236**.